ACS Catalysis

Research Article

pubs.acs.org/acscatalysis

Understanding Selectivity for the Electrochemical Reduction of Carbon Dioxide to Formic Acid and Carbon Monoxide on Metal Electrodes

Jeremy T. Feaster,[†,‡] Chuan Shi,[†,‡] Etosha R. Cave,[†] Toru Hatsukade,[†,‡] David N. Abram,[†] Kendra P. Kuhl,[†] Christopher Hahn,[†,‡] Jens K. Nørskov,[†,‡] and Thomas F. Jaramillo*[,†,‡]

[†]Department of Chemical Engineering, Stanford University, Stanford, California 94305, United States

[‡]SUNCAT Center for Interface Science and Catalysis, SLAC National Accelerator Laboratory, Menlo Park, California 94025, United States

Supporting Information

ABSTRACT: Increases in energy demand and in chemical production, together with the rise in CO_2 levels in the atmosphere, motivate the development of renewable energy sources. Electrochemical CO_2 reduction to fuels and chemicals is an appealing alternative to traditional pathways to fuels and chemicals due to its intrinsic ability to couple to solar and wind energy sources. Formate ($HCOO^-$) is a key chemical for many industries; however, greater understanding is needed regarding the mechanism and key intermediates for $HCOO^-$ production. This work reports a joint experimental and theoretical investigation of the electrochemical reduction of CO_2 to $HCOO^-$ on polycrystalline Sn surfaces, which have been identified as promising catalysts for selectively producing $HCOO^-$. Our results show that Sn electrodes produce $HCOO^-$, carbon monoxide (CO), and hydrogen (H_2) across a range of potentials and that $HCOO^-$ production becomes favored at potentials more negative than −0.8 V vs RHE, reaching a maximum Faradaic efficiency of 70% at −0.9 V vs RHE. Scaling relations for Sn and other transition metals are examined using experimental current densities and density functional theory (DFT) binding energies. While *COOH was determined to be the key intermediate for CO production on metal surfaces, we suggest that it is unlikely to be the primary intermediate for $HCOO^-$ production. Instead, *OCHO is suggested to be the key intermediate for the CO_2RR to $HCOO^-$ transformation, and Sn's optimal *OCHO binding energy supports its high selectivity for $HCOO^-$. These results suggest that oxygen-bound intermediates are critical to understand the mechanism of CO_2 reduction to $HCOO^-$ on metal surfaces.

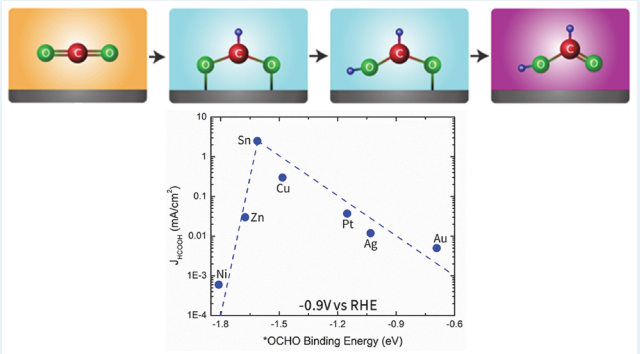

KEYWORDS: *CO_2 reduction, electrocatalysis, tin, Sn, formate, carbon monoxide*

INTRODUCTION

With large increases in CO_2 concentrations in the atmosphere and its detrimental effect on the global environment,[1] it is paramount that viable means of capturing, storing, and converting carbon dioxide be developed.[2] While carbon sequestration and storage (CCS) technologies have advanced greatly in recent years,[3,4] there remains a demand for feasible pathways for converting CO_2 into useful fuels and chemicals.[5] The electrochemical conversion of CO_2 into fuels and chemicals is promising because electroreduction of CO_2 can occur at atmospheric pressures and temperatures, making it ideal for large-scale implementation and integration.[6−8] Partnering electrochemical CO_2 conversion technologies to renewable energy sources could generate carbon-neutral fuels that could be appealing alternatives to fossil fuels. Furthermore, converting CO_2 into commodity chemicals could serve as a carbon sink by sequestering the CO_2 in the atmosphere into ethylene,[9] acetic acid,[10] and formic acid,[11] all of which are produced globally at the commercial scale.

While research over the past several decades has shown that the CO_2 electroreduction reaction (CO_2RR) can occur on various metals and produce a host of products,[12−14] selectivity to particular fuels and chemicals remains a challenge. Furthermore, it has been widely reported that on low roughness factor polycrystalline metal catalysts large overpotentials (>500 mV) are required in order to reach moderate CO_2 reduction selectivity and activity.[12,15] Of these products, formate ($HCOO^-$) is a valuable two-electron product used in a variety of industries and whose production has increased greatly in the past 10 years.[11] Sn electrodes have emerged as attractive candidates for CO_2 reduction on a large scale,[16−18] given the

Received: March 1, 2017
Revised: May 10, 2017
Published: June 22, 2017

DOI: 10.1021/acscatal.7b00687
ACS Catal. 2017, 7, 4822−4827

relative abundance of Sn in the Earth's crust[19] and high selectivity for CO_2 reduction to formate ($HCOO^-$).[16,17,20−23] The selectivity for $HCOO^-$ on Sn and other formate-producing catalysts has yet to be fully determined.

Several possibilities have been represented in the literature for how Sn reduces CO_2 to $HCOO^-$. Early CO_2 studies proposed that $HCOO^-$ could be made via a one-electron transfer to CO_2, forming a $CO_2^{\bullet-}$ radical anion[24−26] that would exist freely in solution; a subsequent proton transfer from water would form $HCOO^{\bullet}$, and a second electron transfer results in the $HCOO^-$ product. Experimental works on Sn electrodes have used Tafel slopes to support this mechanism,[16,18] suggesting that the initial one-electron transfer to $CO_2^{\bullet-}$ is the rate-limiting step in the reaction. Recent theoretical calculations have proposed that $HCOO^-$ production occurs through proton-coupled electron transfer (PCET) on the electrode surface[27,28] and that $HCOO^-$ production on a variety of metal surfaces can occur through both the *COOH and *OCHO intermediates. To date, many questions remain as to why Sn exhibits a high selectivity for formic acid production in comparison to other CO_2 reduction catalysts.

In this study, the catalytic activity of Sn electrodes is investigated for the CO_2RR in aqueous electrolyte as a function of potential. By comparing the production of $HCOO^-$ on Sn electrodes with that of other metal catalysts active for the CO_2RR, and by performing density functional theory (DFT) calculations to estimate the binding energies of various intermediates on these metal surfaces, we propose a means to understand how Sn is selective for the CO_2RR to $HCOO^-$.

EXPERIMENTAL METHODS

All electrochemical experiments were performed using a continuous flow electrolysis reactor previously reported.[29] The compartments were filled with 0.1 M $KHCO_3$ electrolyte (Sigma-Aldrich, 99.99% metals basis) and constantly purged with CO_2 (5.0, Praxair) at 20 sccm. The pH of the electrolyte was consistently measured to be 6.8 before and after each CO_2RR experiment, and a Ag/AgCl reference electrode (Acumen) was used for all experiments. Finally, the compartments were separated by an anion exchange membrane (Selemion membrane, AMV).

Electrolysis of CO_2 on Sn electrodes were performed using a Biologic VMP3 potentiostat with an electrochemical impedance spectroscopy (EIS) capable channel. The resistance across the cell was measured; for all experiments, 85% of the ohmic loss was compensated by the potentiostat, and the remaining 15% was manually compensated after each experiment. All potentials shown in this work are versus the reversible hydrogen electrode (RHE). Furthermore, experiments using Ar instead of CO_2 to show that CO_2 was the primary reacting species were conducted in a manner similar to that for the CO_2 electrolysis experiments (Figure S1 in the Supporting Information). The quantification of gas and liquid products were performed in a fashion similar to that described in our previous work.[30]

Previous reports show that the activity of Sn for CO_2RR depends greatly on the treatment performed on the surface before electrolysis.[15,16] For this study, a high-purity Sn foil (99.99%) was purchased from Alfa Aesar and mechanically polished. The Sn foils were then electropolished in 0.1 M HCl at a potential of −3.0 V vs a graphite counter electrode placed at a distance of 2 cm from the foil. The foils were then rinsed and inserted into the electrochemical cell. This pretreatment removed all excess oxide from the surface, leaving only a native oxide on the Sn electrodes (Figure S2 in the Supporting Information). This oxide layer was removed in the electrochemical cell via cyclic voltammetry (Figure S3 in the Supporting Information), where a reductive feature at −0.3 V vs RHE was observed. This feature is representative of the reduction of Sn^{2+} to metallic Sn.[31]

Binding energies of adsorbates on the (211) facet of FCC transition metals were obtained from density functional theory (DFT) calculations by Peterson et al.[32] Binding energies of adsorbates on the Sn were calculated using a methodology almost identical with that used for the (211) facet for transition metals—plane-wave periodic DFT calculations performed using the DACAPO code with Vanderbilt ultrasoft pseudopotentials.[33,34] A plane-wave energy cutoff of 340 eV and a density cutoff of 640 eV were used. The RPBE exchange-correlation functional was chosen for compatibility with the (211) facet energies as well as its minimal errors for chemisorption energies.[35] The Brillouin zone was sampled with a 4 × 4 × 1 Monkhorst−Pack *k*-point set.[36] Each slab used a 3 × 3 unit cell with four layers−two layers frozen at the bulk lattice constant and two layers allowed to relax freely.

RESULTS AND DISCUSSION

The selectivity of Sn electrodes toward $HCOO^-$ as a function of potential is depicted in Figure 1. Only hydrogen (H_2), $HCOO^-$, and carbon monoxide (CO) were detected; no further reduced products were observed from the polycrystalline Sn electrodes. The partial current densities of $HCOO^-$ and H_2 (Figure 1A), normalized to the geometric surface area, show

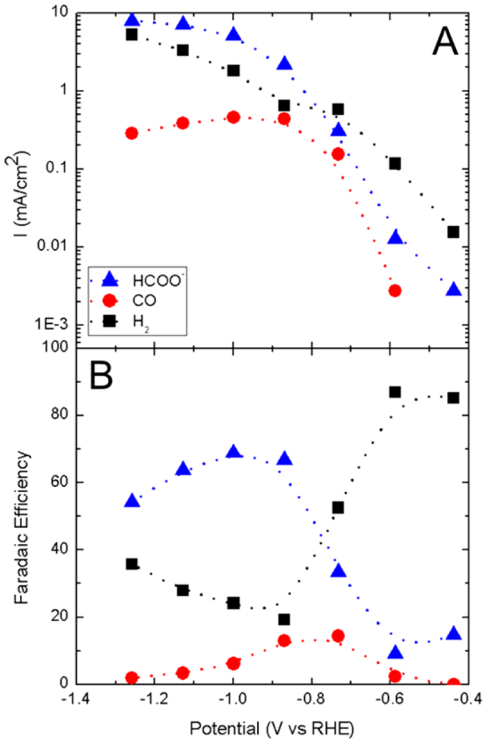

Figure 1. Partial current densities (A) and Faradaic efficiencies (B) for formate, CO, and hydrogen produced on polycrystalline Sn. The Sn electrode is selective toward hydrogen at the earlier overpotentials but becomes selective to formate around −0.8 V vs RHE. A maximum Faradaic efficiency to formate is observed around −0.9 V vs RHE before mass transport of CO_2 becomes the rate-limiting step for CO_2RR.

DOI: 10.1021/acscatal.7b00687
ACS Catal. 2017, 7, 4822−4827

an overall increase in current density as the potential becomes more cathodic. The total Faradaic efficiency for all potentials measured ranged from 90% to 110%. Both H_2 and $HCOO^-$ are first detected at −0.44 V vs RHE with H_2 as the major product, while the first potential where CO is detected is at −0.59 V vs RHE. No products are detected before −0.44 V, and the only Faradaic current measured before this potential is the reduction of the native oxide layer of Sn.[37] $HCOO^-$ becomes the major product at −0.8 V and reaches a maximum Faradaic efficiency of 70% between −0.9 and −1.0 V, whereas CO reaches a maximum Faradaic efficiency of 17% at −0.76 V. As the overpotential increases with potentials more negative than −1.0 V vs RHE, the partial current density for $HCOO^-$ plateaus because, at higher CO_2RR current densities, mass transport becomes limiting. In our electrochemical cell, this mass transport limit is ∼8−10 mA/cm^2 [14] for 2e$^-$ CO_2RR products. Methane, methanol, and other further reduced products were not detected. The electrochemical results are consistent with previous studies on Sn electrodes,[12,15,16,38−40] demonstrating a high selectivity for $HCOO^-$ production.

In light of these results, it is important to consider possible mechanisms and pathways. Tafel slope analysis can be helpful in understanding aspects regarding the hydrogen evolution reaction (HER). Several reports have extrapolated this type of analysis to derive mechanistic information from Sn electrodes,[16,18] particularly on whether the first step is a proton-coupled electron transfer (PCET) or a transfer of one electron to the CO_2 molecule. However, in this work, we focus on gaining insights by directly comparing the CO and $HCOO^-$ production of Sn electrodes to other polycrystalline metal foil catalysts. The CO and $HCOO^-$ partial current densities of the metals selected for this comparison—Ag, Au, Cu, Zn, Pt, and Ni—are taken from our previous studies utilizing the same type of electrochemical cell.[14,29,30] A consistent potential of −0.9 V vs RHE was selected for all metals included in this study; at this potential, only two-electron products (i.e., H_2, CO, $HCOO^-$) are measured on all metals except Cu. Furthermore, this potential is in the kinetic-limited region for each catalyst, allowing for us to analyze the intrinsic activity of each metal without any effect of CO_2 mass transport limitations.

First, we examine the case of CO production. Figure 2 plots the calculated binding energies of *COOH on each metal surface along with each metal's experimentally measured partial current densities toward CO. A trend in activity is observed in the form of a volcano plot for CO_2RR to CO. The Sabatier principle, which states that binding to key intermediates that is neither too strong nor too weak leads to maximum activity, is evident in Figure 2. This volcano plot is very similar to those in previous reports[14] using CO* binding energies as a descriptor and further supports the hypothesis that CO_2 reduction to CO proceeds through a carbon-bound *COOH intermediate, supporting the notion of *COOH as a descriptor for CO production. Sn appears on the weak-binding leg of the volcano due to its weak interaction with COOH*, suggesting that CO_2RR to CO on Sn occurs through a pathway similar to that hypothesized on transition metals.[27,41]

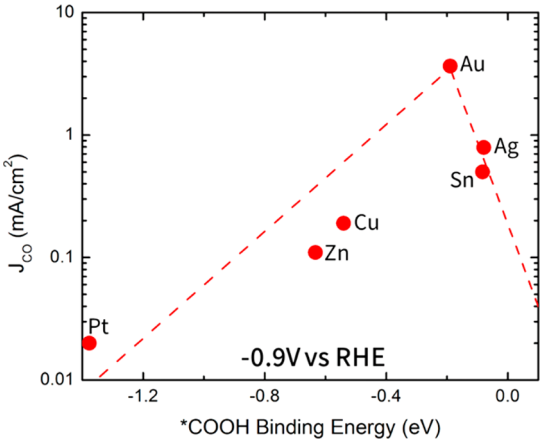

Figure 2. Volcano plot using *COOH binding energy as a descriptor for CO partial current density at −0.9 V vs RHE. Sn appears on the weak-binding leg of the volcano, suggesting that *COOH binding energy is a key intermediate for CO_2 reduction to CO on Sn.

A similar approach was utilized to understand the key intermediate for $HCOO^-$ production. Using *COOH binding energies as a descriptor, the partial current densities of $HCOO^-$ have been plotted (Figure S4 in the Supporting Information). No clear volcano trend is observed, indicating that *COOH may not be the key intermediate for $HCOO^-$ production. Moreover, metals with similar *COOH binding energies (e.g., Sn and Ag) exhibit vastly different partial current densities for $HCOO^-$, which is unexpected if *COOH is the main intermediate for CO_2RR to $HCOO^-$. As no correlation is observed between *COOH binding energies and $HCOO^-$ activity, *COOH binding energy is not likely the key descriptor for the reduction of CO_2 to $HCOO^-$, unlike the case for CO production.

Figure 3 plots $HCOO^-$ partial current densities at −0.9 V vs RHE versus *OCHO binding energies instead, to establish whether $HCOO^-$ production proceeds through an oxygen-bound intermediate. Indeed, a clear volcano trend is observed among all (Figure 3). Au, Ag, Pt, and Cu are on the weak-binding side of the volcano, indicating that *OCHO may not interact strongly enough with the surface to lead to high selectivity to $HCOO^-$. Ni and Zn are on the strong-binding side of the volcano, indicating that *OCHO binds too strongly to the surface for further reduction to formate. Sn appears near the top of this volcano, implying that Sn has a near-optimal binding energy of the key intermediate *OCHO to produce

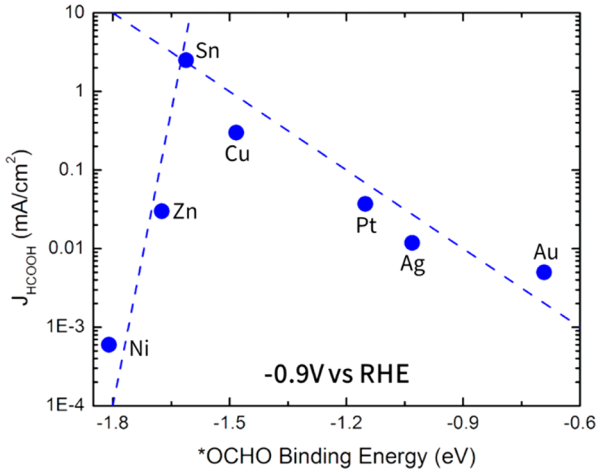

Figure 3. Volcano plot using *OCHO binding energy as a descriptor for $HCOO^-$ partial current density at −0.9 V vs RHE. Sn appears near the top of the volcano, suggesting that *OCHO is a key intermediate for CO_2 reduction to $HCOO^-$ on Sn.

DOI: 10.1021/acscatal.7b00687
ACS Catal. 2017, 7, 4822−4827

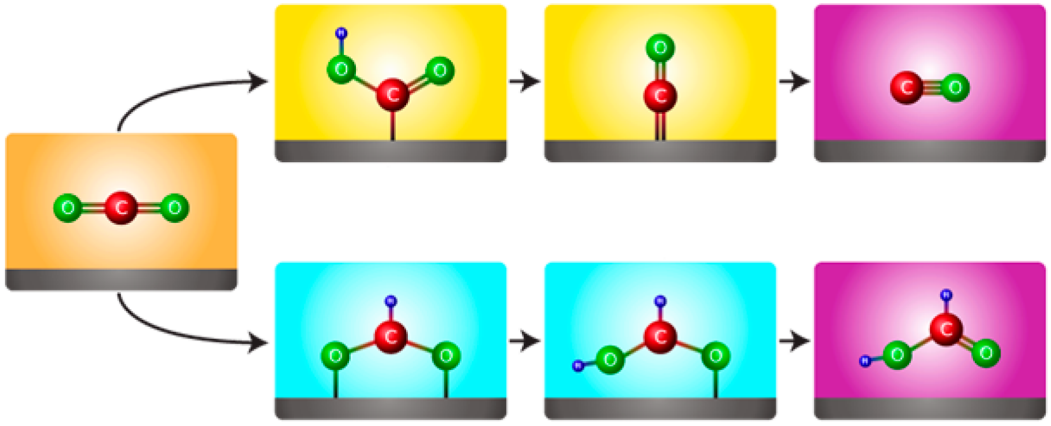

Figure 4. Mechanism that includes pathways for CO and $HCOO^-$ production from CO_2. CO_2 may bind to the electrode surface in an initial electrochemical step via the carbon or the oxygens (resulting in a single adsorption intermediate, *COOH, or a bidentate *OCHO intermediate, respectively). The second electrochemical step results in the production of CO or $HCOO^-$. For metals that are far from the optimal *OCHO binding energy but near the optimal *COOH binding energy, it is possible that *COOH may be the intermediate for $HCOO^-$ production.

$HCOO^-$. This volcano suggests that *OCHO is a key intermediate for $HCOO^-$ production on transition metals as well as Sn and provides an explanation for Sn's high selectivity toward $HCOO^-$. While *OCHO has been suggested as a possible intermediate for $HCOO^-$ production on Cu[42] and other metals,[28] no other experimental work to date has established *OCHO as the primary intermediate for $HCOO^-$ production on a wide range of metals or proposed a possible explanation for Sn's selectivity to $HCOO^-$.

Several additional insights can be obtained from Figures 2 and 3 about metal selectivity toward $2e^-$ products (i.e., H_2, CO, and $HCOO^-$). For the metals that are not near the peaks of the *COOH and *OCHO volcanos (e.g., Pt, Ni), the major product being produced at −0.9 V vs RHE is H_2; this is unsurprising, as neither of these catalysts have optimal binding energies for either $HCOO^-$ or CO production. With regard to the CO_2RR, both Pt and Ni produce more $HCOO^-$ than CO. As both Pt and Ni have a very strong binding affinity for carbon-bound intermediates such as *COOH and *CO, it is likely that CO poisons the metal surface and limits the amount of CO produced on these electrodes. For the metals that are not near the peak of the *OCHO volcano but near the peak of the *COOH volcano (e.g., Au, Ag), the major product being produced at −0.9 V vs RHE is CO, with only a small amount of $HCOO^-$ being detected. This suggests that, although the *COOH binding energies for most of the metals in this study are weaker in comparison to *OCHO, kinetic limitations that are not captured in the electronic energy calculations might play a nontrivial role in determining selectivity for these metals. For instance, metal cation interactions on Au and Ag could alter the electrode surface in a way that would lead to lower barriers for *COOH adsorption,[43] limiting the production of $HCOO^-$ and leading to the high selectivity of CO. For these metals with low binding affinity to oxygen but near-optimal carbon binding affinity, it appears that the *COOH pathway to CO is preferable to the *OCHO pathway to $HCOO^-$. From these observations, it seems that, regardless of *COOH binding energy, if a metal is not near the peak of the *OCHO volcano, $HCOO^-$ production is greatly reduced in comparison to other $2e^-$ products.

However, for the metals that are near the peak of the *OCHO volcano but not near the peak of the *COOH volcano (e.g., Cu, Zn), the major product formed on these surfaces is H_2. Furthermore, on Zn the major CO_2RR product is CO, whereas the major CO_2RR product on Cu is $HCOO^-$. Zn could be limited in its production of $HCOO^-$ due to its very strong *OCHO binding energy, which could lead to a higher Faradaic efficiency for hydrogen evolution. While it has been shown that Zn binds CO very weakly,[14] Zn has an intermediate *COOH binding energy due to a bidentate interaction with the surface. Both carbon and oxygen binding energies play a role in determining *COOH binding energy on Zn, which explains why it does not sit on the weak-binding side of the *COOH volcano. Cu, having an intermediate *COOH binding energy and sitting on the weak-binding side of the *OCHO volcano, also produces methane and ethylene at this potential. On the basis of these results, Cu binds *OCHO weakly enough for $HCOO^-$ production to not dominate the CO_2RR (although it is the major CO_2RR product at this potential) but has an intermediate *COOH binding energy to the surface for further reduced products to be observed. Along with a high overpotential for the hydrogen evolution reaction,[27,28] Cu seems to have a combination of binding energies that enables it to produce $>2e^-$ products. For the metals that are near the peak of both the *COOH and *OCHO volcanoes (e.g., Sn, In), the major product formed on the electrode surface is $HCOO^-$ (Figures S5 and S6 in the Supporting Information). For Sn, the *OCHO pathway for $HCOO^-$ production dominates over the *COOH pathway for CO production. The *OCHO volcano suggests that oxygen-bound intermediates interact more strongly with the Sn surface than carbon-bound intermediates and steer Sn's selectivity to $HCOO^-$ over CO.

These results suggest that, for the metals shown in Figures 2 and 3, CO production occurs primarily through a key carbon-bound intermediate, *COOH, and $HCOO^-$ production proceeds primarily through a key oxygen-bound intermediate, *OCHO. It is important to consider both *COOH and *OCHO binding energies for these pathways, as the two energies do not scale (Figure S7 in the Supporting Information). Figures 2 and 3 underscore the importance of both carbon and oxygen affinities for understanding the CO_2RR. Additionally, these results are consistent with recent operando spectroscopic techniques that have reported observing *OCHO on Sn electrodes.[40,44] While it has been suggested that $HCOO^-$ could be generated through the *COOH intermediate,[28] particularly on transition-metal surfaces with

DOI: 10.1021/acscatal.7b00687
ACS Catal. 2017, 7, 4822−4827

very low binding affinity to *OCHO (e.g., Au, Ag), our results do not indicate any relationship between *COOH binding energy and $HCOO^-$ production (Figure S4 in the Supporting Information).

From a combination of the insights gained from the *COOH and *OCHO volcanoes, a mechanism for CO_2RR to $2e^-$ products is presented in Figure 4. The first PCET can take place either on one of the oxygens, resulting in a carbon-bound COOH* (top path), or on the carbon atom, resulting in an oxygen-bound OCHO* (bottom path). The second electrochemical step for the top and bottom paths leads directly to *CO and *HCOOH, respectively. The final step of desorption results in either CO or $HCOO^-$ being released from the surface of the electrode. These results provide new insights into the CO_2RR on metal catalysts to $2e^-$ products.

CONCLUSIONS

We have reported the catalytic activity of Sn electrodes for CO_2 reduction as a function of potential. Using an electrochemical cell designed for high sensitivity to identify and quantify the products of the CO_2RR, we note that the only products observed are H_2, CO, and $HCOO^-$. $HCOO^-$ was confirmed as the major CO_2RR product formed on Sn and was the dominant product over H_2 at potentials more negative than −0.8 V vs RHE. We have compared the production of CO and $HCOO^-$ on Sn to that of other metals to examine trends in behavior. DFT calculated *COOH binding energy emerges as a descriptor for the CO_2RR to CO, resulting in a clear volcano trend and suggesting that *COOH is a key intermediate for CO production. However, *COOH binding energies do not describe $HCOO^-$ production across the metals in this study, suggesting that $HCOO^-$ does not primarily proceed through this carbon-bound intermediate. Instead, we find that *OCHO binding energies accurately describe the behavior of the CO_2RR to $HCOO^-$ across the range of metals, resulting in a clear volcano trend. Furthermore, Sn is located near the top of the volcano, indicating that it has a near-optimal *OCHO binding energy for the production of $HCOO^-$. These results underscore the importance of surface oxophilicity in describing the activity and selectivity of metal catalysts for CO_2 reduction. Establishing trends in CO and $HCOO^-$ production that incorporate the appropriate descriptors is helpful for designing catalysts that can achieve high selectivity to $HCOO^-$, CO, and other products of interest.

ASSOCIATED CONTENT

Supporting Information

The Supporting Information is available free of charge on the ACS Publications website at DOI: 10.1021/acscatal.7b00687.

HCO_3^- reduction experiments, SEM of poly-Sn and XPS before/after pretreatment, CV and CAs of CO_2RR on Sn, $HCOO^-$ production vs *COOH binding energy, *COOH volcano including In, *OCHO volcano including In, and *OCHO binding energy vs *COOH binding energy (PDF)

AUTHOR INFORMATION

Corresponding Author

*E-mail for T.F.J.: jaramillo@stanford.edu.

ORCID

Christopher Hahn: 0000-0002-2772-6341

Thomas F. Jaramillo: 0000-0001-9900-0622

Notes

The authors declare no competing financial interest.

ACKNOWLEDGMENTS

This material is based upon work supported by the National Science Foundation CAREER Award No. 1066515 and by the Global Climate & Energy Project (GCEP) at Stanford University. The DFT calculations performed were funded by the Air Force Office of Scientific Research (AFOSR) through the Multidisciplinary University Research Initiative (MURI) under AFOSR Award No. FA9550-10-1-0572. J.T.F. acknowledges support by a National Science Foundation Graduate Research Fellowship. The authors also thank Joshua Willis for his help with Figure 4. Thanks are due to Dr. Stephen R. Lynch of the Stanford Department of Chemistry NMR facility for his help with the 600 and 500 MHz experiments.

REFERENCES

(1) Karl, T. R.; Trenberth, K. E. *Science* **2003**, *302*, 1719−1723.

(2) Hoffert, M. I.; Caldeira, K.; Benford, G.; Criswell, D. R.; Green, C.; Herzog, H.; Jain, A. K.; Kheshgi, H. S.; Lackner, K. S.; Lewis, J. S.; Lightfoot, H. D.; Manheimer, W.; Mankins, J. C.; Mauel, M. E.; Perkins, L. J.; Schlesinger, M. E.; Volk, T.; Wigley, T. M. *Science* **2002**, *298*, 981−987.

(3) D'Alessandro, D. M.; Smit, B.; Long, J. R. *Angew. Chem., Int. Ed.* **2010**, *49*, 6058−6082.

(4) Pires, J. C. M.; Martins, F. G.; Alvim-Ferraz, M. C. M.; Simões, M. *Chem. Eng. Res. Des.* **2011**, *89*, 1446−1460.

(5) Whipple, D. T.; Kenis, P. J. A. *J. Phys. Chem. Lett.* **2010**, *1*, 3451−3458.

(6) Costentin, C.; Robert, M.; Saveant, J. M. *Chem. Soc. Rev.* **2013**, *42*, 2423−2436.

(7) Lu, Q.; Rosen, J.; Zhou, Y.; Hutchings, G. S.; Kimmel, Y. C.; Chen, J. G.; Jiao, F. *Nat. Commun.* **2014**, *5*, 3242.

(8) Agarwal, A. S.; Zhai, Y.; Hill, D.; Sridhar, N. *ChemSusChem* **2011**, *4*, 1301−1310.

(9) True, W. R. *Oil and Gas Journal* **2012**, *110*, 78−84.

(10) Le Berre, C.; Serp, P.; Kalck, P.; Torrence, G. P. *Ullmann's Encyclopedia of Industrial Chemistry* **2013**, 1−34.

(11) Reutemann, W.; Kieczka, H. *Ullmann's Encyclopedia of Industrial Chemistry* **2011**, 1.

(12) Hori, Y.; et al. *Electrochim. Acta* **1994**, *39*, 1833−1839.

(13) Gattrell, M.; Gupta, N.; Co, A. *J. Electroanal. Chem.* **2006**, *594*, 1−19.

(14) Kuhl, K. P.; Hatsukade, T.; Cave, E. R.; Abram, D. N.; Kibsgaard, J.; Jaramillo, T. F. *J. Am. Chem. Soc.* **2014**, *136*, 14107−14113.

(15) Jitaru, M.; Lowy, D. A.; Toma, M.; Toma, B. C.; Oniciu, L. *J. Appl. Electrochem.* **1997**, *27*, 875−889.

(16) Chen, Y.; Kanan, M. W. *J. Am. Chem. Soc.* **2012**, *134*, 1986−1989.

(17) Machunda, R. L.; Ju, H.; Lee, J. *Curr. Appl. Phys.* **2011**, *11*, 986−988.

(18) Prakash, G. K. S.; Viva, F. A.; Olah, G. A. *J. Power Sources* **2013**, *223*, 68−73.

(19) Vesborg, P. C. K.; Jaramillo, T. F. *RSC Adv.* **2012**, *2*, 7933−7947.

(20) Anawati; Frankel, G. S.; Agarwal, A.; Sridhar, N. *Electrochim. Acta* **2014**, *133*, 188−196.

(21) Bumroongsakulsawat, P.; Kelsall, G. H. *Electrochim. Acta* **2014**, *141*, 216−225.

(22) Wu, J.; Harris, B.; Sharma, P. P.; Zhou, X. D. *ECS Trans.* **2013**, *58*, 71−80.

(23) Li, Y.; Qiao, J.; Zhang, X.; Lei, T.; Girma, A.; Liu, Y.; Zhang, J. *ChemElectroChem* **2016**, *3*, 1618−1628.

(24) Hori, Y.; Suzuki, S. *Bull. Chem. Soc. Jpn.* **1982**, *55*, 660−665.

(25) Jordan, J.; Smith, P. T. *Proc. Chem. Soc.* **1960**, 246−247.

DOI: 10.1021/acscatal.7b00687
ACS Catal. 2017, 7, 4822−4827

(26) Paik, W.; Andersen, T. N.; Eyring, H. *Electrochim. Acta* **1969**, *14*, 1217−1232.
(27) Peterson, A. A.; Abild-Pedersen, F.; Studt, F.; Rossmeisl, J.; Nørskov, J. K. *Energy Environ. Sci.* **2010**, *3*, 1311−1315.
(28) Yoo, J. S.; Christensen, R.; Vegge, T.; Norskov, J. K.; Studt, F. *ChemSusChem* **2016**, *9*, 358−363.
(29) Kuhl, K. P.; Cave, E. R.; Abram, D. N.; Jaramillo, T. F. *Energy Environ. Sci.* **2012**, *5*, 7050−7059.
(30) Hatsukade, T.; Kuhl, K. P.; Cave, E. R.; Abram, D. N.; Jaramillo, T. F. *Phys. Chem. Chem. Phys.* **2014**, *16*, 13814−13819.
(31) BARONETTI, G.; de Miguel, S. R.; et al. *Appl. Catal.* **1986**, *24*, 109−116.
(32) Peterson, A. A.; Nørskov, J. K. *J. Phys. Chem. Lett.* **2012**, *3*, 251−258.
(33) Vanderbilt, D. *Phys. Rev. B: Condens. Matter Mater. Phys.* **1990**, *41*, 7892−7895.
(34) Center for Atomicscale Materials Design (CAMD), Technical University of Denmark, Lyngby, Denmark.
(35) Hammer, B.; Hansen, L.; Nørskov, J. *Phys. Rev. B: Condens. Matter Mater. Phys.* **1999**, *59*, 7413−7421.
(36) Monkhorst, H. J.; Pack, J. D. *Phys. Rev. B* **1976**, *13*, 5188−5192.
(37) Takeno, N. *AIST Today (Jpn. Ed.)* **2005**, 241−243.
(38) Zhang, S.; Kang, P.; Meyer, T. J. *J. Am. Chem. Soc.* **2014**, *136*, 1734−1737.
(39) Wu, J.; Risalvato, F. G.; Ke, F. S.; Pellechia, P. J.; Zhou, X. D. *J. Electrochem. Soc.* **2012**, *159*, F353−F359.
(40) Baruch, M. F.; Pander, J. E.; White, J. L.; Bocarsly, A. B. *ACS Catal.* **2015**, *5*, 3148−3156.
(41) Shi, C.; Hansen, H. A.; Lausche, A. C.; Norskov, J. K. *Phys. Chem. Chem. Phys.* **2014**, *16*, 4720−4727.
(42) Durand, W. J.; Peterson, A. A.; Studt, F.; Abild-Pedersen, F.; Nørskov, J. K. *Surf. Sci.* **2011**, *605*, 1354−1359.
(43) Chen, L. D.; Urushihara, M.; Chan, K.; Nørskov, J. K. *ACS Catal.* **2016**, *6*, 7133−7139.
(44) Dutta, A.; Kuzume, A.; Rahaman, M.; Vesztergom, S.; Broekmann, P. *ACS Catal.* **2015**, *5*, 7498−7502.

DOI: 10.1021/acscatal.7b00687
ACS Catal. 2017, 7, 4822−4827